Atomic scale trap state characterization by dynamic tunneling force microscopy

R. Wang,[1] S. W. King,[2] and C. C. Williams[1,a)]
[1]*Department of Physics and Astronomy, University of Utah, Salt Lake City, Utah 84112, USA*
[2]*Logic Technology Development, Intel Corporation, Hillsboro, Oregon 97124, USA*

(Received 17 June 2014; accepted 6 July 2014; published online 5 August 2014)

Dynamic tunneling force microscopy (DTFM) is applied to the study of point defects in an inter-layer dielectric film. A recent development enables simultaneous acquisition of DTFM, surface potential, and topographic images while under active height feedback control. The images show no clear correlation between trap state location and surface potential or topography of the surface. The energy and depth of individual trap states are determined by DTFM images obtained at different probe tip heights and applied voltages and quantitative tunneling and electrostatic models. The measured density of states in these films is found to be approximately $1 \times 10^{19}\,cm^{-3}\,eV^{-1}$ near the dielectric film surface. © *2014 AIP Publishing LLC*. [http://dx.doi.org/10.1063/1.4890966]

Electron trap states are found in dielectric materials and influence their electronic properties and performance in device structures.[1] For example, low-k inter-layer dielectric (ILD) films[2] are used to separate metal lines between electronic devices to ensure a high operational speed of the circuit. Reliability of these materials is a major concern, as electronic trap states play a role in film leakage and breakdown.[3–5] Significant work has been done in characterizing such defect states using electron spin resonance (ESR),[6,7] electrically detected magnetic resonance (EDMR),[8] conductance and capacitance techniques,[9] and by measuring de-trapping current following photo-excitation.[10,11] However, these macroscopic methods only probe the ensemble of trap states. As semiconductor devices march toward single digit nanometer dimensions, an atomic scale understanding of individual defect states and the role they play in these materials is needed.[12]

Electrical properties of dielectric films have been characterized using scanning probe microscopy (SPM) methods, such as scanning tunneling microscopy (STM),[13] conductive atomic force microscopy (c-AFM),[14] ballistic electron emission microscopy (BEEM),[15] Kelvin probe force microscopy (KPFM),[16] electrostatic force microscopy (EFM),[17] and scanning capacitance microscopy (SCM).[18] Among these, STM, c-AFM, and BEEM are limited by the requirement that a detectable current must be achieved and therefore they apply only to dielectric films with adequate conductance. KPFM and EFM can only measure charged trapping sites rather than neutral states. Atomic scale SCM imaging has not been achieved due to either finite probe tip radius or limited sensitivity.

Dynamic tunneling force microscopy (DTFM)[19] is based upon single electron tunneling between an AFM probe tip and a single trap state near the sample surface.[20,21] The electron tunneling is detected by the electrostatic force the charge produces on the probe tip, providing a method to detect and image electron trap states in completely non-conductive surfaces. The spatial resolution of the method benefits from the exponential dependence of tunneling rate with gap, as in scanning tunneling microscopy, and therefore atomic scale imaging can be achieved. The first DTFM images were obtained using a constant probe height mode (no probe height feedback). To achieve high quality DTFM images, however, the tip-sample gap must be maintained constant to within a fraction of a nanometer during the acquisition of an image, which typically takes a few minutes. Reducing the tip-sample thermal drift and piezoelectric creep to a fraction of a nanometer per image is difficult and time consuming. Additionally, imaging in constant height mode does not work on surfaces that are not atomically flat. Operating with AFM probe height feedback eliminates both issues and allows images to be acquired over long time periods.

A method to provide height feedback control during DTFM imaging has been developed which facilitates acquisition of full images with a constant tip-sample gap. To achieve this, it is necessary to implement a KPFM feedback loop[22] to null the electrical field between tip and surface. This helps to keep the cantilever frequency shift (df) independent of surface potential variations, so that df can be used to keep the tip-sample gap constant. Keeping the tip at the same potential as the local surface also provides a useful reference for energy measurements, as described below. Moreover, two additional channels of simultaneous information (surface potential and topography) are provided by the improved method. Correlation of the three independent channels provides additional physical understanding of the dielectric film and the trap states observed.

Figure 1 shows the DTFM experimental set-up. Measurements are performed with an Omicron Multiprobe S atomic force microscope under a vacuum of 10^{-10} mBar at room temperature. A metal coated AFM probe (NanosensorPPP-NCHPt), with ~10 nm tip oscillation amplitude and ~40 N/m stiffness is brought within tunneling range of a dielectric surface. A periodic asymmetric square wave shuttling voltage at ~300 Hz is applied to the sample with tip grounded, consisting of a positive voltage ($+V_{ac}$) for 77% of its duty cycle and a negative voltage ($-V_{ac}$) for

a)Electronic mail: clayton@physics.utah.edu

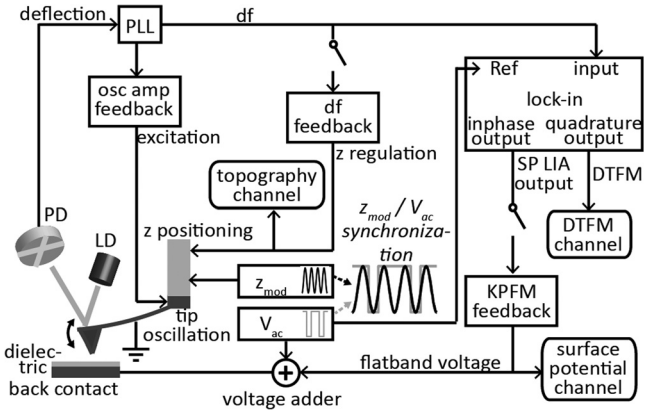

FIG. 1. Block diagram of the DTFM with height and Kelvin probe force microscopy feedback control. z_{mod} is a sinusoidal modulation applied to the probe tip height and V_{ac} is an asymmetric square wave voltage applied to the sample. Synchronization of the z_{mod} and V_{ac} are shown above. The in-phase output signal of the lock-in amplifier (with V_{ac} as reference) is denoted as the surface potential lock-in amplifier output (SP LIA output), to differentiate from surface potential signal, which in this paper denotes the KPFM feedback voltage applied to the sample (to keep the tip and sample at flat band). The photodiode, laser diode, phase lock loop, and oscillation amplitude are denoted as PD, LD, PLL, and osc amp, respectively.

the remaining 23%. The tip height is also modulated sinusoidally (z_{mod}) with a 2 nm amplitude at twice the shuttling voltage frequency. Waveforms of voltage and height modulations are synchronized as shown in Figure 1. The cantilever frequency shift (df) signal goes to a two phase lock-in amplifier which is referenced with the shuttling voltage. The in-phase and quadrature phase components of the frequency shift (df) signal at 300 Hz are both measured. The in-phase component corresponds to the local surface potential of the sample, which is kept at zero via a KPFM feedback loop, and the quadrature phase component of df is the DTFM signal. The average frequency shift (df) is used to control tip height during scanning.

The DTFM method without height and KPFM feedback is explained in detail in Ref. 19. Briefly, the square wave shuttling voltage is applied to move the tip Fermi level between a high and a low level with respect to the trap states in the surface. This induces electrons to tunnel to and from these states. The height modulation is to bring the tip into and out of tunneling range. This causes the electron tunneling (shuttling) to occur with a phase that is approximately 90° out of phase with surface potential signal. If a trap state is at a depth that is within tunneling range and also has an energy between the high and low tip Fermi level positions, an electron will shuttle between the tip and the state at the frequency of the shuttling voltage. This electron shuttling causes a periodic electrostatic force gradient on the probe, which is detected as a periodic frequency shift of the probe oscillation frequency. This frequency shift is detected by a lock-in amplifier in quadrature with the applied shuttling voltage.

The sample utilized in this study is a 6 nm low-k ILD film (k = 3.3) a-$SiO_{1.2}C_{0.35}$:H fabricated at Intel Corporation by plasma enhanced chemical vapor deposition (PECVD). Details concerning film deposition process can be found in Ref. 23. The sample was ultrasonically cleaned both in acetone and isopropyl alcohol for 15 min, then rinsed in deionized water and blown dry with nitrogen gas. The sample was then inserted in the UHV chamber and heated at 380 °C for 1 h to desorb water and organic contaminants from ambient exposure.

DTFM images are acquired on a $(50\,nm)^2$ area of the ILD sample surface at various tip-surface gaps (z_{min}) and shuttling voltages (V_{ac}) (See Figs. 2(a)–2(h)). The tip-sample gap is determined by pulling the tip back a known distance from the position at which the df-z curve reaches a minimum value.[21]

As the tip is scanned laterally across a trap state accessible by tunneling, an electron will shuttle between the tip and state and the DTFM signal increases. Each bright region in the DTFM image therefore represents an individual electron trap state. The DTFM image is a two dimensional map of the trap states accessible to tunneling in the dielectric surface. The apparent size of each bright region may be much larger than the true spatial extent of the trap states, as the size is determined by a tip imaging effect.[19] The apparent size of a given trap state is influenced by its depth, the tip height, and the shape of the probe apex (see Figure 2(k)).

The surface potential image (Fig. 2(i)) and topography image (Fig. 2(j)) in this sample region are simultaneously acquired with the DTFM image (Fig. 2(c)). Comparison of the DTFM, surface potential, and topography images shows that there is little correlation between the trap state locations (bright spots in DTFM image) and local surface potential or topography. There is a slowly varying background observed in the DTFM image, which does appear to be correlated with the corresponding surface potential image. This correlation is currently under study. Note that there is also a weak DTFM-like signal which appears in the surface potential image at the trap state locations of DTFM image. This is due to the fact that when electron shuttling occurs, there is a small average surface potential shift caused by the additional average surface charge in the state (½ electron) due to the electron shuttling.[24]

Figure 2 also shows a comparison between DTFM images at different tip-sample gaps (z_{min}) and applied voltages (V_{ac}). As V_{ac} increases (Figs. 2(a)–2(d)) at constant z_{min}, new states appear while the previously observed states remain. This can be explained by the fact that as V_{ac} is increased, a larger energy range of trap states are being accessed, due to the larger movement of the tip Fermi level. As z_{min} decreases (Figs. 2(f)–2(i)) at constant V_{ac}, more states appear because states deeper in the film are accessible to tunneling as tip moves closer to surface.

The energy and depth of trap states accessible by DTFM with a given V_{ac} and z_{min} are calculated using an electrostatic and tunneling model from Ref. 25. (Figure 3). Some improvements have been made to more accurately account for tip motion.[24] The depth of the states accessible to tunneling is determined by the tunneling barrier, which includes the barrier in the gap and in the film, for those states at a finite depth. The barrier height in the film depends on the trap state energy. The energies accessible by tunneling are determined by the shuttling voltage (V_{ac}). Accessibility to tunneling is calculated numerically for a grid of points in energy/depth space for given z_{min} and V_{ac}. In the tunneling rate calculations,[26] the following physical parameters have been used: electron effective mass (0.5 times electron mass in

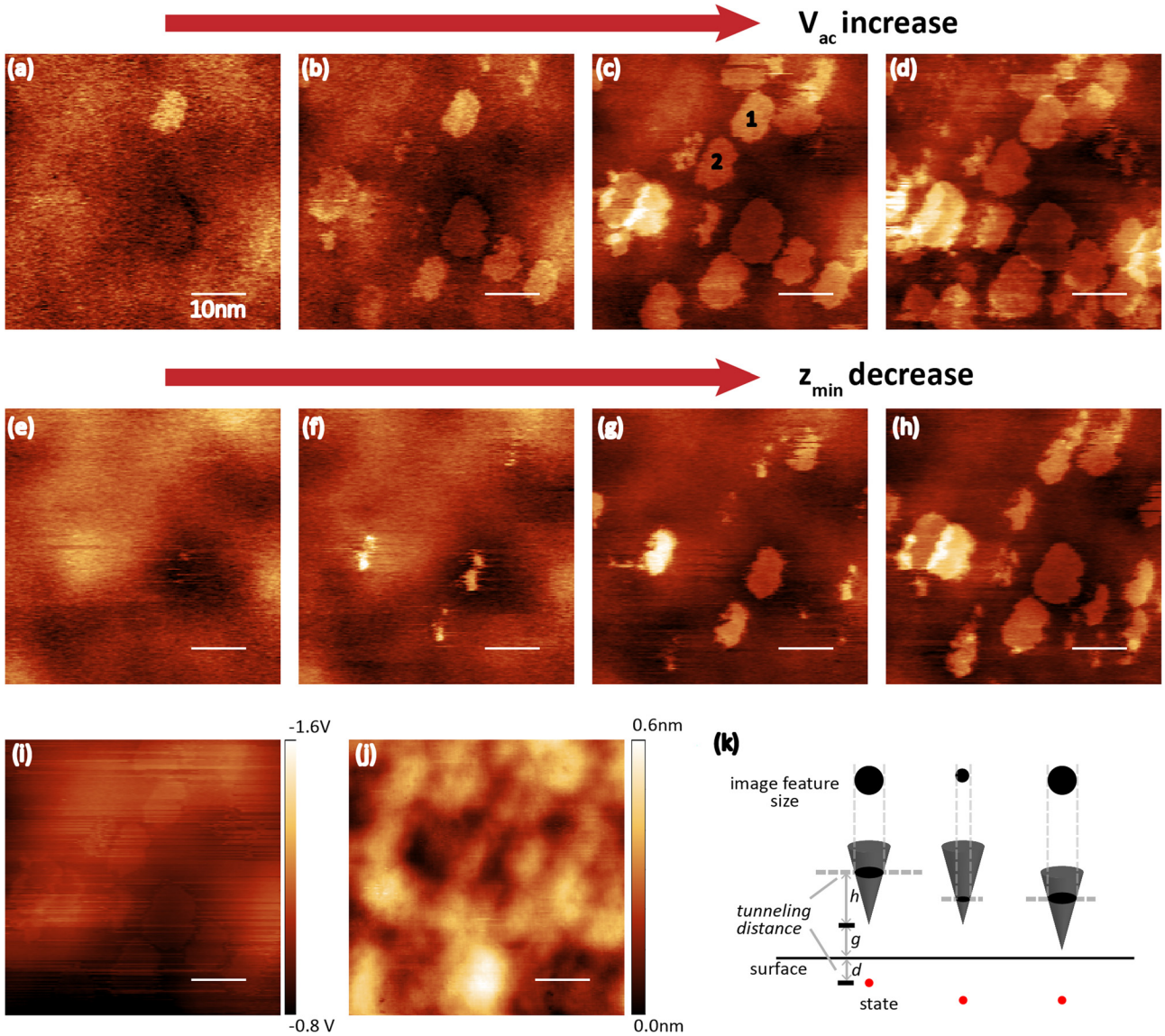

FIG. 2. (a)–(h) are DTFM images taken in the same sample area at different tip-surface gaps (z_{min} is the smallest tip-sample gap during tip height modulation) and shuttling voltages (V_{ac}). The scale bar is 10 nm in all images. (a) $z_{min} = 0.5$ nm, $V_{ac} = 0.5$ V; (b) $z_{min} = 0.5$ nm, $V_{ac} = 1$ V; (c) $z_{min} = 0.5$ nm, $V_{ac} = 2$ V; (d) $z_{min} = 0.5$ nm, $V_{ac} = 3$ V; (e) $z_{min} = 1.3$ nm, $V_{ac} = 3$ V; (f) $z_{min} = 1.1$ nm, $V_{ac} = 3$ V; (g) $z_{min} = 0.9$ nm, $V_{ac} = 3$ V; (h) $z_{min} = 0.7$ nm, $V_{ac} = 3$ V. The color scale is chosen independently in each image for best contrast. Two particular states are identified by numbers 1 and 2 in (c). (i) is a surface potential image. (j) is a topography image. Both (i) and (j) are simultaneously acquired with the DTFM image (c). (k) illustrates the principle behind the apparent size of the trap states in the DTFM images. d is the trap state depth in the film, g is the tip-sample gap, and h is the height above the tip apex from which tunneling to a particular state can occur.

vacuum[27]), platinum tip work function (5.4 eV (Ref. 28)), platinum tip Fermi energy relative to bottom of band (8.5 eV), dielectric film electron affinity (0.7 eV (Ref. 29)), and band gap (8.2 eV (Ref. 23)). The tip Fermi level under the flat band condition is assigned to be zero energy in Figs. 3 and 4 (on left vertical axis), which is equivalent to 3.5 eV above the dielectric valence band (right vertical axis of Fig. 4). Since we actively keep the surface and tip at flat band during DTFM imaging, energies of the states can be determined unambiguously with respect to dielectric energy bands as long as band structure of the tip and dielectric are known. From Fig. 3, we can see that as V_{ac} increases, more states in a larger energy range become accessible, and as z_{min} decreases, deeper states become accessible.

Each individual state observed in the images shown in Figure 2 can be assigned to a particular region of energy-depth space by differentially subtracting the regions calculated for different z_{min} and V_{ac}.[25] In Figure 4, each energy/depth region is identified by different colors. For example, state 1 in Figure 2(c) has an average depth of 0.13 nm and average energy of 3.5 eV above the dielectric valence band, and state 2 has an average depth of 0.15 nm and an average energy of either 3.2 eV or 3.8 eV. The energy ambiguity for state 2 is reflected in Fig. 4 by the fact that regions of the same color are found both above and below 3.5 eV (right axis). This ambiguity comes from the fact that an AC voltage is used to shuttle the electron, and only the magnitude of the trap state energy relative to the tip Fermi level at flat band can be determined. In the future, this ambiguity will be eliminated by performing single electron tunneling force spectroscopy (frequency shift versus voltage curves)[30] over each observed state in the DTFM images. The finite resolution of

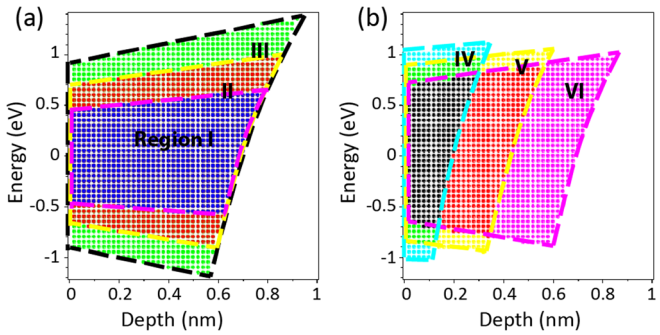

FIG. 3. Calculated regions of energy and depth accessible by DTFM at different shuttling voltages and probe heights. Numerical calculation of tunneling probability leads to a grid of points showing tunneling accessible energies and depths. Approximate boundary lines are drawn to guide the eye. (a) Region I corresponds to a $z_{min} = 0.5$ nm and $V_{ac} = 2$ V, region II: $z_{min} = 0.5$ nm and $V_{ac} = 3$ V, and region III: $z_{min} = 0.5$ nm and $V_{ac} = 4$ V; (b) Region IV: $V_{ac} = 3$ V and $z_{min} = 0.9$ nm, region V:$V_{ac} = 3$ V and z_{min} 0.7 nm, and region VI: $V_{ac} = 3$ V and $z_{min} = 0.5$ nm (same as region II in (a)).

the energy and depth determination is due to the finite intervals of z_{min} and V_{ac} chosen in experiment. The uncertainty in tip/surface gap determination of $\sim(\pm 0.15\,\text{nm})$ leads to a depth uncertainty of ± 0.2 nm and an energy uncertainty of $\pm(0.1\,\text{eV})$ in the energy-depth measurements.

Using the data obtained with the maximum V_{ac} applied voltage (+/−3 V) and minimum gap z_{min} (0.5 nm) to image this sample, the average density of states between ~2.5 eV and ~4.5 eV above the dielectric valence mobility edge and within ~0.8 nm depth of the surface is determined to be $1 \times 10^{19}\,\text{cm}^{-3}\,\text{eV}^{-1}$. This direct measurement of the density of states is unique in that it does not depend on the state's initial charge occupation or spin. The method also provides a direct determination of the real space distribution of states.

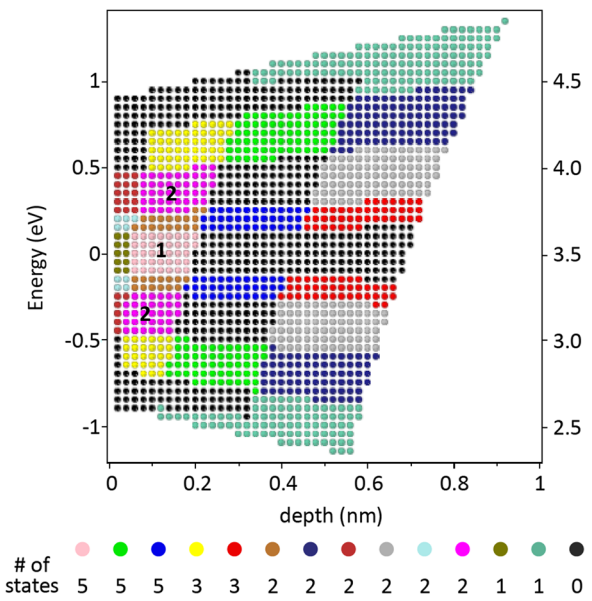

FIG. 4. Differential energy-depth regions calculated for the states shown in the images of Figure 2 (Data from an additional DTFM image with $z_{min} = 0.5$ nm, $V_{ac} = 4$ V are not shown in Fig. 2). The energy axis on the left is relative to tip Fermi level at flatband and the energy axis on the right is relative to dielectric valence mobility edge. State 1 and 2 identified in Figure 2(c) are found to fall into the pink and magenta energy/depth regions in Fig. 4. The color table at the bottom of the figure records how many states (of 35 observed) fall into each differential region of energy-depth space identified by a color.

It is noteworthy that in this particular film, the density of states is not uniformly distributed with respect to energy or depth. For example, in Fig. 4 there are 8 of 35 total states that are concentrated in the adjoining green and yellow areas, and another 8 states located in the adjoining blue and red areas, but no states in any of the black regions. This quantitative measure of the density of trap states is not easily determined by other methods. Further improvements to the methodology will provide a unique quantitative determination of the energy and depth of every individual state accessible to tunneling.

In summary, dynamic tunneling force microscopy measurements are performed on an interlayer dielectric film with height and surface potential feedback control, providing images of trap state distribution, surface potential, and topography. The images indicate that little correlation exists between the trap state locations and the local surface potential or topography of the film. The energy and depth of the trap states are calculated using a tunneling model. The average density of states is quantitatively determined to be $1 \times 10^{19}\,\text{cm}^{-3}\,\text{eV}^{-1}$ near the dielectric surface and in the energy range from 2.5 to 4.5 eV above the valence edge. This direct measurement of the spatial distribution and average density of trap states will be useful in understanding dielectric materials needed for future device applications.

The authors would like to thank the Semiconductor Research Corporation for funding this work.

[1]*Solid-State Physics: An Introduction to Principles of Materials Science*, edited by H. Ibach and H. Luth, 4th ed. (Springer, 2009), Chap. 11.
[2]K. Maex, M. R. Baklanov, D. Shamiryan, S. H. Brongersma, and Z. S. Yanovitskaya, J. Appl. Phys. **93**, 8793 (2003).
[3]K. Y. Yiang, W. J. Yoo, Q. Guo, and A. Krishnamoorthy, Appl. Phys. Lett. **83**, 524 (2003).
[4]J. M. Atkin, T. M. Shaw, E. Liniger, R. B. Laibowitz, and T. F. Heinz, in IEEE International Reliability Physics Symposium (IRPS) (IEEE, 2012), p. BD-1.
[5]G. G. Gischia, K. Croes, G. Groeseneken, Z. Tokei, V. Afanas'ev, and L. Zhao, in IEEE International Reliability Physics Symposium (IRPS) (IEEE, 2010), pp. 549–555.
[6]B. C. Bittel, P. M. Lenahan, and S. W. King, Appl. Phys. Lett. **97**, 063506 (2010).
[7]H. Ren, M. T. Nichols, G. Jiang, G. A. Antonelli, Y. Nishi, and J. L. Shohet, Appl. Phys. Lett. **98**, 102903 (2011).
[8]C. J. Cochrane and P. M. Lenahan, Appl. Phys. Lett. **104**, 093503 (2014).
[9]J. M. Atkin, E. Cartier, T. M. Shaw, R. B. Laibowitz, and T. F. Heinz, Appl. Phys. Lett. **93**, 122902 (2008).
[10]J. M. Atkin, D. Song, T. M. Shaw, E. Cartier, R. B. Laibowitz, and T. F. Heinz, J. Appl. Phys. **103**, 094104 (2008).
[11]H. Sinha, H. Ren, M. T. Nichols, J. L. Lauer, M. Tomoyasu, N. M. Russell, G. Jiang, G. A. Antonelli, N. C. Fuller, S. U. Engelmann, Q. Lin, V. Ryan, Y. Nishi, and J. L. Shohet, J. Appl. Phys. **112**, 111101 (2012).
[12]S. King, H. Simka, D. Herr, H. Akinaga, and M. Garner, APL Mater. **1**, 40701 (2013).
[13]M. E. Welland and R. H. Koch, Appl. Phys. Lett. **48**, 724 (1986).
[14]T. Ruskell, R. Workman, D. Chen, D. Sarid, S. Dahl, and S. Gilbert, Appl. Phys. Lett. **68**, 93 (1996).
[15]B. Kaczer, Z. Meng, and J. P. Plez, Phys. Rev. Lett. **77**, 91 (1996).
[16]R. Ludeke and E. Cartier, Appl. Phys. Lett. **78**, 3998 (2001).
[17]L. J. Klein and C. C. Williams, Appl. Phys. Lett. **81**, 4589 (2002).
[18]Y. Naitou, H. Arimura, N. Kitano, S. Horie, T. Minami, M. Kosuda, H. Ogiso, T. Hosoi, T. Shimura, and H. Watanabe, Appl. Phys. Lett. **92**, 012112 (2008).
[19]J. P. Johnson, N. Zheng, and C. C. Williams, Nanotechnology **20**, 055701 (2009).
[20]E. Bussmann, D. J. Kim, and C. C. Williams, Appl. Phys. Lett. **85**, 2538 (2004).

[21]E. Bussmann, N. Zheng, and C. C. Williams, Appl. Phys. Lett. **86**, 163109 (2005).
[22]W. Melitz, J. Shen, A. C. Kummel, and S. Lee, Surf. Sci. Rep. **66**, 1 (2011).
[23]S. King, B. French, and E. Mays, J. Appl. Phys. **113**, 44109 (2013).
[24]R. Wang and C. C. Williams, "Dynamic Tunneling Force Microscopy for atomic scale imaging and characterization of electronic defect states" (unpublished).
[25]J. P. Johnson, D. W. Winslow, and C. C. Williams, Appl. Phys. Lett. **98**, 052902 (2011).
[26]N. Zheng, C. C. Williams, E. G. Mishchenko, and E. Bussmann, J. Appl. Phys. **101**, 093702 (2007).
[27]J. Borja, J. L. Plawsky, T. M. Lu, H. Bakhru, and W. N. Gill, J. Appl. Phys. **115**, 084107 (2014).
[28]C. Kim, J. Korean Phys. Soc. **47**, 417 (2005).
[29]H. Zheng, S. W. King, V. Ryan, Y. Nishi, and J. L. Shohet, Appl. Phys. Lett. **104**, 062904 (2014).
[30]E. Bussmann and C. C. Williams, Appl. Phys. Lett. **88**, 263108 (2006).